Supporting Information:

Fast Hydrogen Atom Abstraction by a Hydroxo Iron(III) Porphyrazine

Hongxin Gao and John T. Groves*

Department of Chemistry, Princeton University, Princeton New Jersey 08544, United States

jtgroves@princeton.edu

Materials and Methods

2,3-Pyridinedicarboxylic acid, urea, ferrous chloride tetrahydrate, ammonium heptamolybdate tetrahydrate, methyl *p*-toluenesulfonate, ammonium hexafluorophosphate, tetra-*n*-butylammonium bromide, perchloric acid, phosphoric acid, sodium phosphate monobasic, sodium hydroxide, dimethyl sulfoxide, methanol, diethyl ether, isopropyl alcohol, acetone, and acetonitrile were purchased from Sigma-Aldrich and used without further purification. Xanthene, 9,10-dihydroanthracene, fluorene, triphenylmethane and diphenylmethane were obtained from Sigma-Aldrich and purified by recrystallization. D_2O was obtained from Cambridge Isotope Laboratories, Inc. Water used in all experiments was deionized (Millipore, Milli-Q). Phosphate buffer solutions were prepared by mixing H_3PO_4 and NaH_2PO_4 in water and the pH was adjusted with NaOH.

Instrumentation

UV-vis spectral measurements were made with a Hewlett-Packed 8453 diode array spectrophotometer at room temperature, with a 10 mm path quartz cuvette. Stopped-flow experiments were performed with a Hi-Tech SF-61DX2 double mixing instrument with a 10 mm path length, or a SF-61SX2 single mixing instrument with a 2 mm path length, equipped with an ISOTEMP 1016S thermostat bath. NMR spectra were recorded on a 500 MHz Bruker Avance-III spectrometer. EPR experiments were recorded on a Bruker Elexsys 580 X-band CW-EPR system. GC-MS analyses were performed on an Agilent 7890A gas chromatograph equipped with an Agilent 5975 mass selective detector. High-resolution mass spectra were obtained by electrospray ionization (ESI) on an Agilent 6220 LC-TOF spectrometer. Electrochemical measurements were performed on a BAS 100B electrochemical workstation at room temperature using a Ag/AgCl reference electrode, a glassy carbon working electrode, and a Pt auxiliary electrode. Solution pH was measured using an Accumet AB15 pH electrode from Fisher Scientific, and calibrated (pH 4.0, 7.0, and 10.0) prior to use.

Synthesis and purification of $(PyPz)Fe^{II}(OH_2)_2$ (2)

Synthesis and purification of **2** were adapted from reported procedures.[1] Pyridine-2,3-dicarboxylic acid (668 mg, 4 mmol), ferrous chloride tetrahydrate (199 mg, 1 mmol), urea (961 mg, 16 mmol) and ammonium heptamolybdate tetrahydrate (12 mg, 0.01 mmol) were heated together in an uncapped round bottom flask at 180 ℃ for 30 min. Upon cooling to RT, the resulting solid was washed with water, acetone and methanol on a glass filter. This crude iron 2,3-pyridinoporphyrazine was then added to a solution of DMSO (7 mL) and methyl *p*-toluenesulfonate (5.0 g) and heated at 70 ℃ for 24 h.

After the reaction, the cooled mixture was added 250 mL of chloroform, causing Fe^{II}PyPz (*p*-toluenesulfonate salt) to precipitate. This product was filtered on a glass filter and washed with acetone before being pulled through with methanol. Excess ammonium hexafluorophosphate was then added to the methanol solution, causing the hexafluorophosphate salt of **2** to precipitate. The resulting solid was then filtered and washed with a mixture of 50/50 (v/v) isopropanol/diethyl ether before being pulled through with acetone. Excess tetra-*n*-butylammonium bromide (TBA-Br) was added to the acetone solution, causing the bromide salt of **2** to precipitate. This purified salt was then isolated by filtration and washed with excess acetone, until no $(C_4H_9)_4N^+$ ion could be detected by ESI-MS. The dark green to black solid, $[Fe^{II}PyPz]^{4+}[4Br^-]$, **2**, was obtained in 21% overall yield. The chloride salt, $[Fe^{II}PyPz]^{4+}[4Cl^-]$, was also prepared using the same procedure with tetra-*n*-butylammonium chloride replacing TBA-Br. The chloride salt of FePyPz had the same UV-Vis absorption, pK_a, NMR and same redox behavior as the bromide salt of FePyPz. Reaction kinetics were also the same for both the bromide and chloride salts of FePyPz.

^{1}H NMR (500 MHz, D_2O): δ 10.36 (4H, m), 9.37 (4H, m), 8.56 (4H, m), 5.92 (12H, m). ESI-MS: calculated $C_{32}H_{24}FeN_{12}^+$: 632.1591, found 632.1583. Elemental analysis ($C_{32}H_{24}N_{12}FeBr_4 \cdot 2H_2O$): C calculated 38.90, found 39.39; H calculated 2.86, found 3.07; Br calculated 32.35, found 31.35.

Reaction Kinetics

For kinetic measurements, (PyPz)$Fe^{II}(OH_2)_2$ tetra bromide (**2**) was dissolved in aqueous solution and the pH adjusted to 2.2 either with 6 mM perchloric acid (unbuffered) or with 100 mM phosphate/phosphoric acid buffer. The mixture was electrolyzed at 1000 mV vs. Ag/AgCl to generate (PyPz)$Fe^{III}(OH)(OH_2)$ (**1**), unless stated otherwise. The resulting aqueous solution of **1** was then mixed with equal volume of acetonitrile and was used to fill one syringe of the stopped-flow instrument. The other syringe was filled with substrate, which was dissolved in the same 50/50 (v/v) aqueous/acetonitrile solvent. Acetonitrile was added in order to increase the solubility of organic substrates. These steps were performed quickly to limit spontaneous decay of **1** back to **2** (~5 min half-life). Each experiment was repeated at least three times. Concentrations presented are the final concentrations after mixing. Kinetic data were obtained in single-mixing mode (with either a double-mixing instrument or single-mixing instrument) using diode array detection. Spontaneous decay of **1** back to **2** ($k \sim 0.0024\ s^{-1}$) was slow with respect to these kinetic analyses. Values of k_{obs} were processed by fitting the kinetic profile to a single exponential equation using Kinetic Studio from Hi-Tech. Global and SVD (singular value decomposition) analyses were analyzed by ReactLab™ Kinetics from Jplus Consulting. Values of second-order rate constants were obtained from the slope of a k_{obs} vs. the [substrate] plot. Global analyses gave first-order rate constants within 2% of the corresponding k_{obs} calculated by single wavelength techniques. SVD analyses gave two components accounting for more than 98.6% of all values for all kinetic measurements, indicating only two observable species varying during the kinetic measurements.

Product analyses

For product analyses, (PyPz)$Fe^{II}(OH_2)_2$ (**2**) (0.5 mM) was dissolved in aqueous solution (pH 2.2 using either 6 mM perchloric acid (unbuffered) or with 100 mM phosphate/phosphoric acid buffer). and electrolyzed at 1000 mV vs. Ag/AgCl to generate (PyPz)$Fe^{III}(OH)(OH_2)$ (**1**). Equal molar concentration (to **1**) of substrate was dissolved in acetonitrile and mixed with solution of **1** in 1:1 volume ratio. After all **1** was converted to **2**, the reaction mixture was then extracted with ethyl acetate, dried with sodium sulfate, and analyzed by GC-MS. Starting material and oxidation product are readily detected and compared to authentic standards. Xanthone, anthracene, fluorenone, triphenylmethanol and benzophenone were observed as products of xanthene, dihydroanthracene, fluorene, triphenylmethane and diphenylmethane, respectively.

Synthesis of xanthene-*d*$_2$

Synthesis and purification were adapted from reported procedures.[2] Xanthene (1.82 g, 10 mmol) was dissolved in DMSO-d_6 (10 mL) along with NaH (1.20 g, 50 mmol) under N_2. The reaction mixture was stirred at RT for 2 h, and then quenched with D_2O (10 mL). The crude product was filtered and washed with copious amounts of H_2O. The resulting solid was purified by silica gel column chromatography with hexane eluent, then recrystallized from isopropanol; ^{1}H NMR (500 MHz, $CDCl_3$): δ 7.19 (4H, m), 7.04 (4H, m), 4.05 (0.038H). The NMR data indicated > 98% deuteration. The reported KIE, 20.2, is uncorrected for residual protium in the xanthene-d_2. A protium content of 1% would give a corrected KIE of 25, however, the excellent single-exponential fit for the reduction of **1** by xanthene-d_2 in H_2O ($R^2 = 0.9998$) argues against that much protium in the xanthene-d_2 substrate.

9,10-Dihydroanthracene-d_4 and fluorene-d_2 were prepared by similar methods. Deuteration of fluorene-d_2 and 9,10-dihydroanthracene-d_4 were > 99% and 98%, respectively, as analyzed by ^{1}H NMR.

References

(1) (a) Umile, T. P.; Wang, D.; Groves, J. T., *Inorg. Chem.* **2011**, *50*, 10353. (b) Safari, N.; Jamaat, P. R.; Shirvan, S. A.; Shoghpour, S.; Ebadi, A.; Darvishi, M.; Shaabani, A., *J. Porphyrins Phthalocyanines* **2005**, *9*, 256. (c) Bahadoran, F.; Dialameh, S., *J. Porphyrins Phthalocyanines* **2005**, *9*, 163.

(2) Goldsmith, C. R.; Jonas, R. T.; Stack, T. D. P., *J. Am. Chem. Soc.* **2002**, *124*, 83.

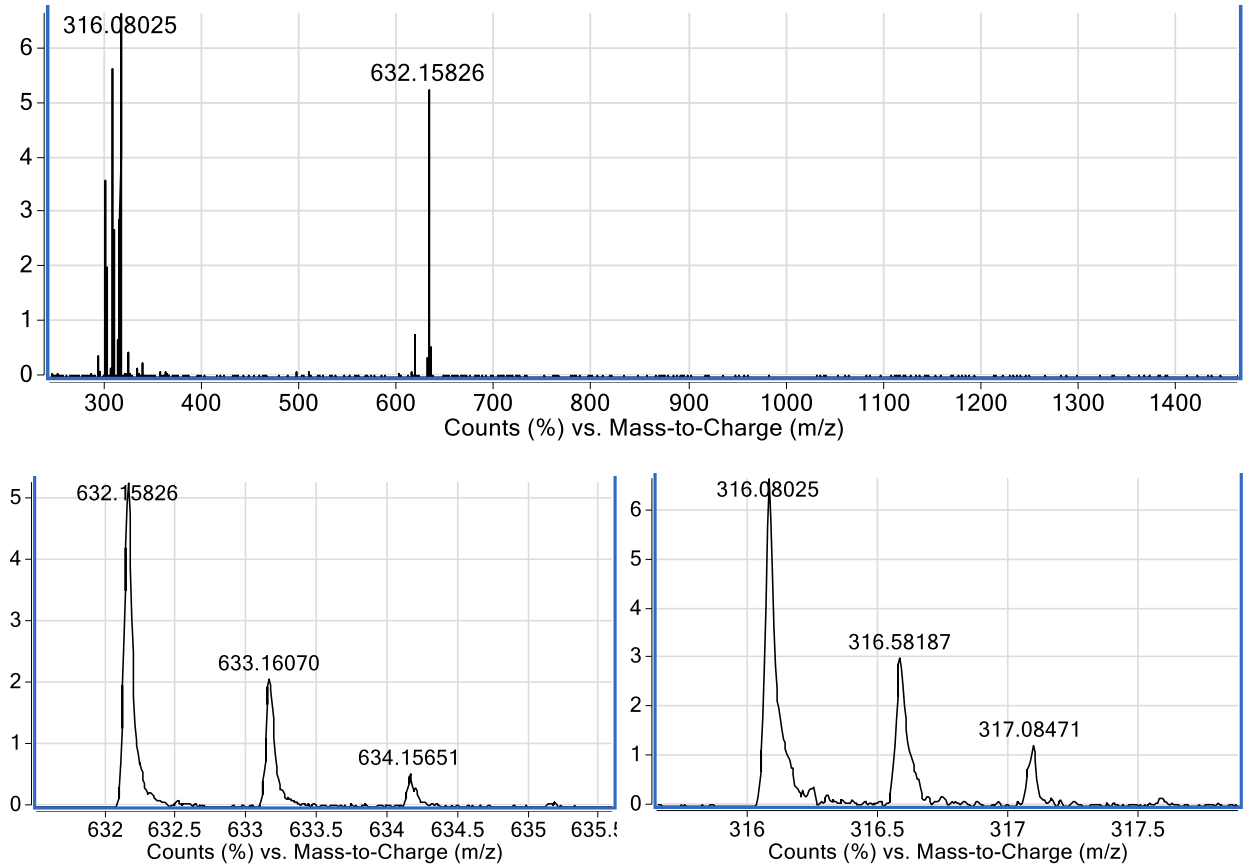

Figure S1. High resolution electrospray ionization mass spectrometry of (PyPz)Fe^{II} (**2**). HR-ESI-MS (flying with one positive charge) for $C_{32}H_{24}FeN_{12}^{+}$: expected 632.1591 m/z, observed 632.1583 m/z. Expected relative isotope intensities: M 100%, M+1 41.4%, M+2 7.3%. Observed relative isotope intensities: M 100%, M+1 40%, M+2 8%. HR-ESI-MS (flying with two positive charges) for $C_{32}H_{24}FeN_{12}^{2+}$: expected 316.0793 m/z, observed 316.0803 m/z. Observed relative isotope intensities: M 100%, M+1 44%, M+2 16%.

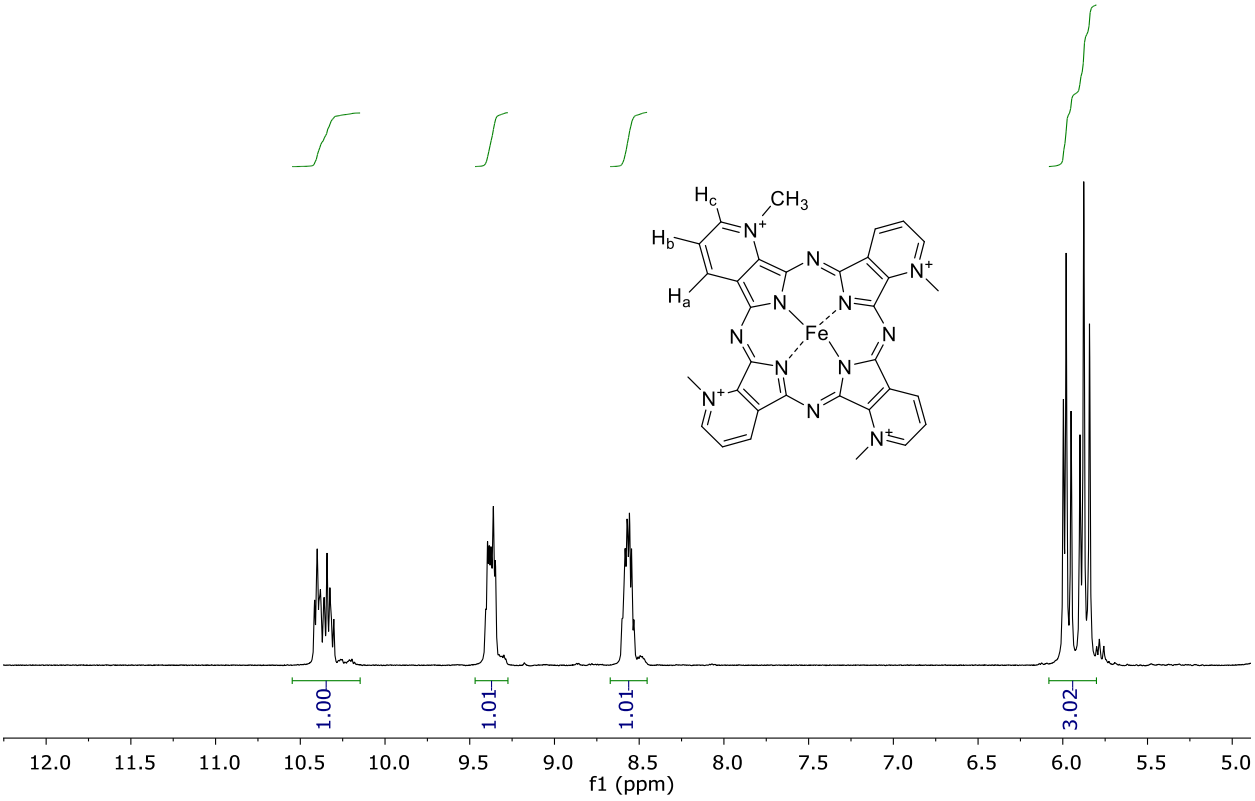

Figure S2. ^{1}H NMR (500 MHz) of (PyPz)Fe^{II} (**2**) in D_2O. δ 10.36 (H_a, m, 4H), δ 9.37 (H_c, m, 4H), δ 8.56 (H_b, m, 4H), δ 5.92 (methyl, m, 12H). The N-methyl region ~δ 6 indicates a near-statistical mixture of regioisomers (cf. reference 15).

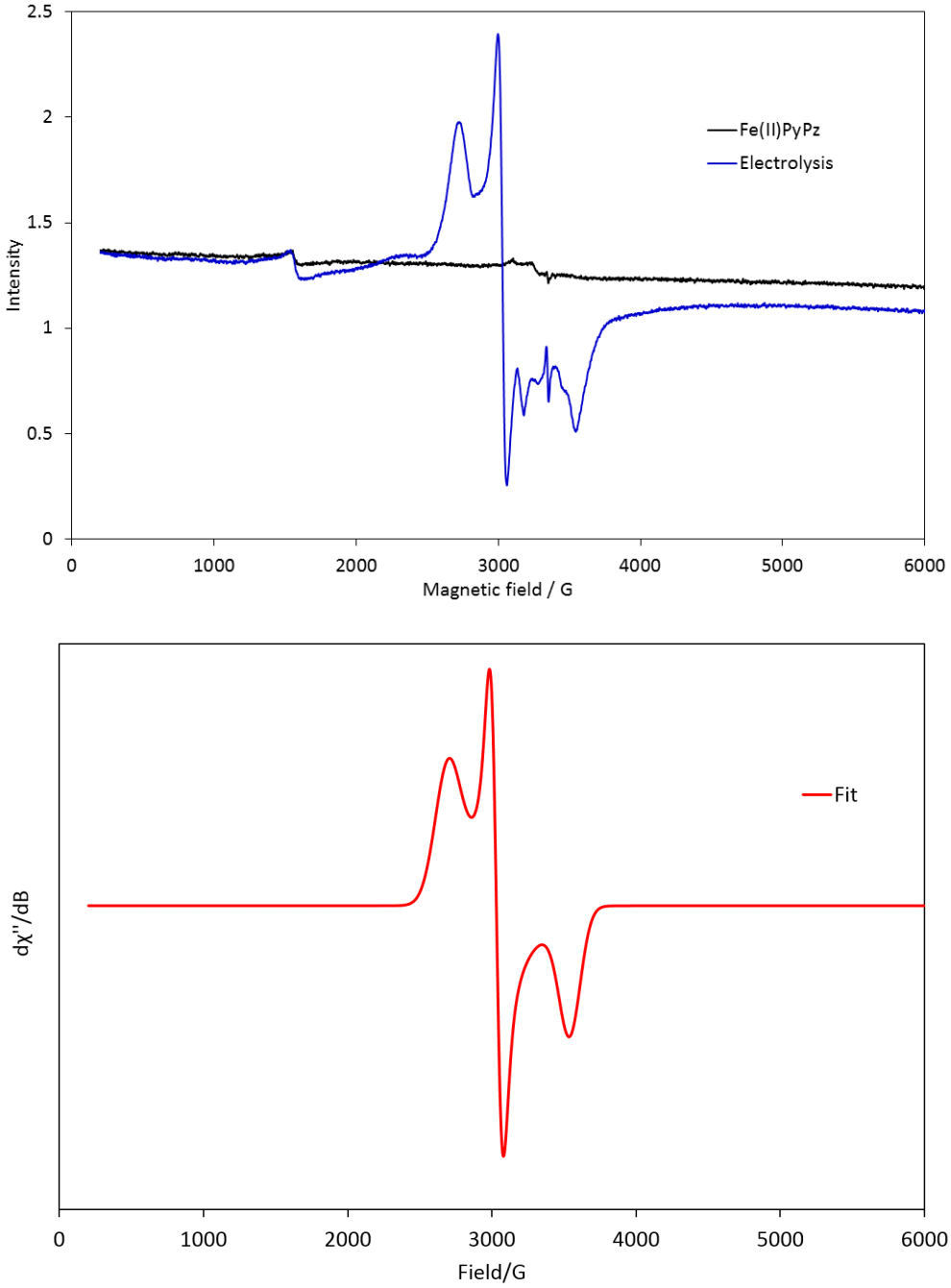

Figure S3. (Upper panel) EPR spectra of (PyPz)Fe^{II} (**2**) and (PyPz)Fe^{III} (**1**) obtained by bulk electrolysis at 1000 mV vs Ag/AgCl. Small feature near g = 4.3 is typical of trace ferric impurities that are common in aqueous buffers. Microwave frequency, 9.4 GHz; microwave power, 2 mW; (PyPz)Fe concentration, 1 mM; solvent, 6 mM $HClO_4$ aqueous solution, pH 2.2; temperature, 10 K. (Lower panel) Fit of EPR of **1** to g = 2.49, 2.21, 1.89. EPR was fit with EasySpin on MATLAB. Fit parameters: Nucleus = Fe, S = ½, g = 2.49, 2.21, 1.89, gStrain = (0, 0, 0.05), A = (0, 4.4, 0.3), AStrain = (0.0017, 0.0054, 0.0030), HStrain = (550, 0, 0), lwpp = (0, 2).

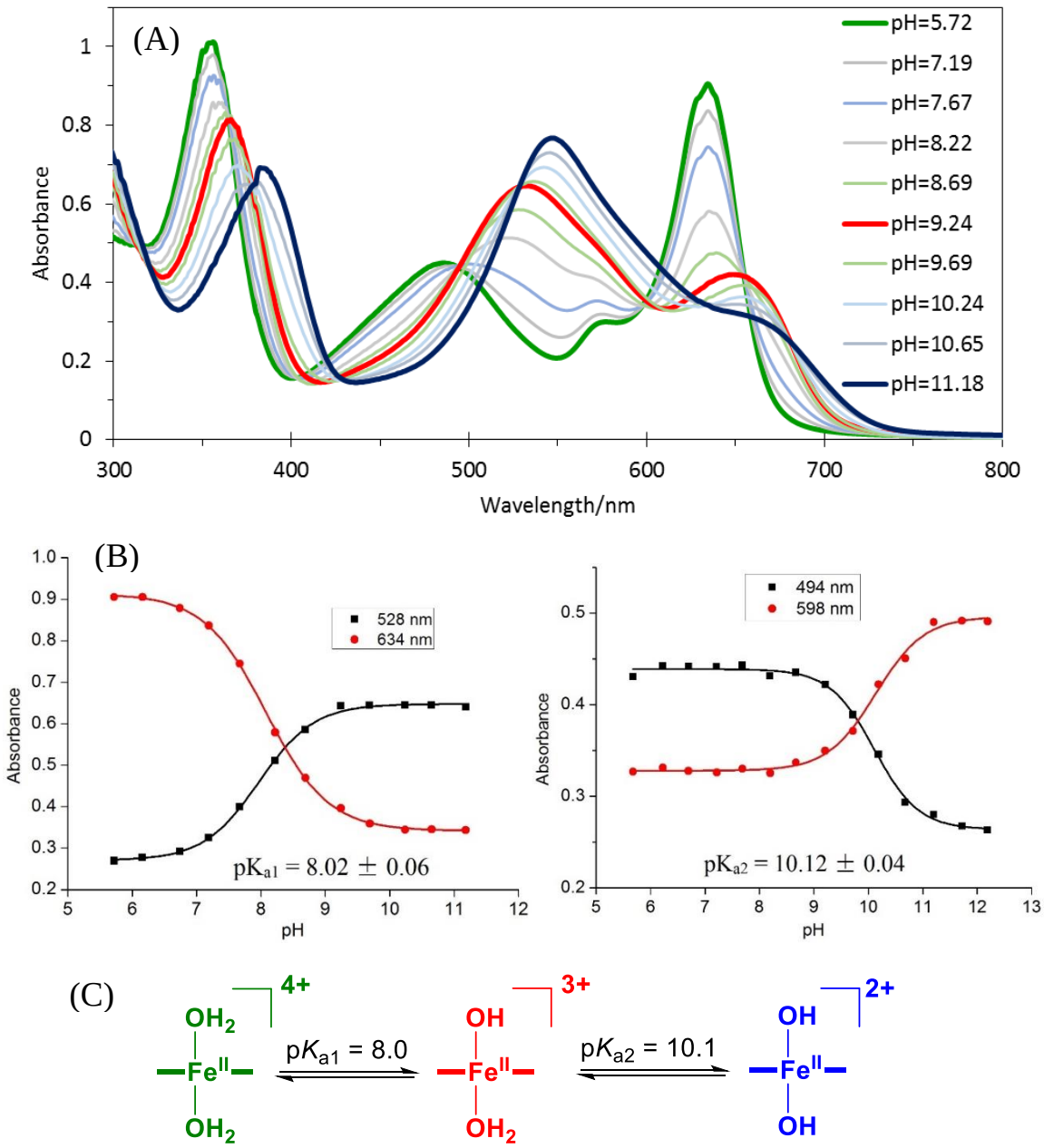

Figure S4. (A) UV-vis spectra of 23 μM (PyPz)Fe^{II} (**2**) in 100 mM sodium phosphate buffer over a range of pH. Isosbestic points are observed at 494 and 598 nm (from pH 5 to 9, right panel of (B)), 528 and 634 nm (from pH 9 to 11, left panel of (B)). SVD analysis indicated that the first three components accounting for > 99% of the variation of the data with pH. (B) Plots of absorbance vs. pH for (PyPz)Fe^{II}; pK_{a1} = 8.02 ± 0.06 and pK_{a2} = 10.12 ± 0.04 calculated from the Henderson-Hasselbalch equation. Global analysis gives pK_{a1} = 8.03 and pK_{a2} = 10.34, consistent with the single wavelength analysis. (C) Diaqua (green), aqua-hydroxo (red) and dihydroxo (blue) speciation of (PyPz)Fe^{II} (**2**). The titration was reversible and give the same pK_a values when the pH was varied from 12 to 5.

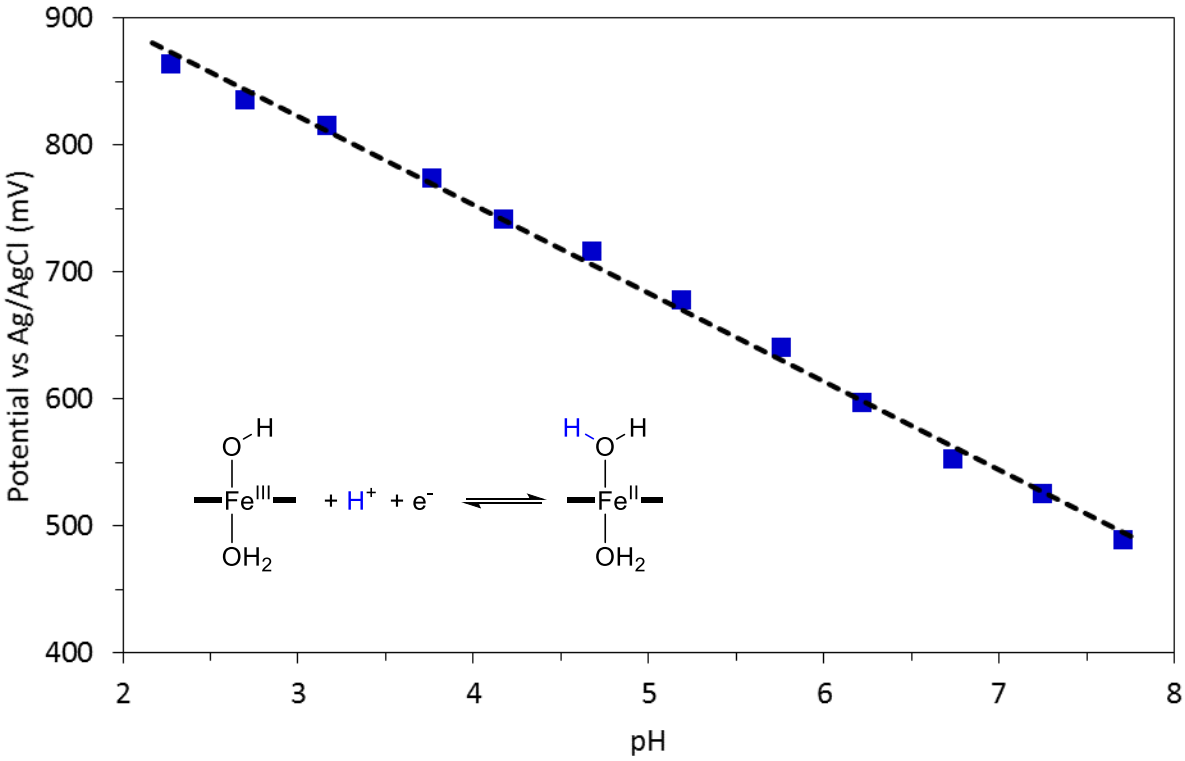

Figure S5. Pourbaix diagram of 1 mM (PyPz)Fe in 100 mM sodium phosphate (NaPi) buffer. Blue squares are $E_{1/2}$ measured by cyclic voltammetry over the pH range from 2.2 to 7.7. The black dashed line is a linear fit of redox potentials vs. pH with a slope of –69 mV/pH (R^2 = 0.997), close to the theoretical –59.1 mV/pH, indicating a one-proton, one-electron redox process over the entire pH range.

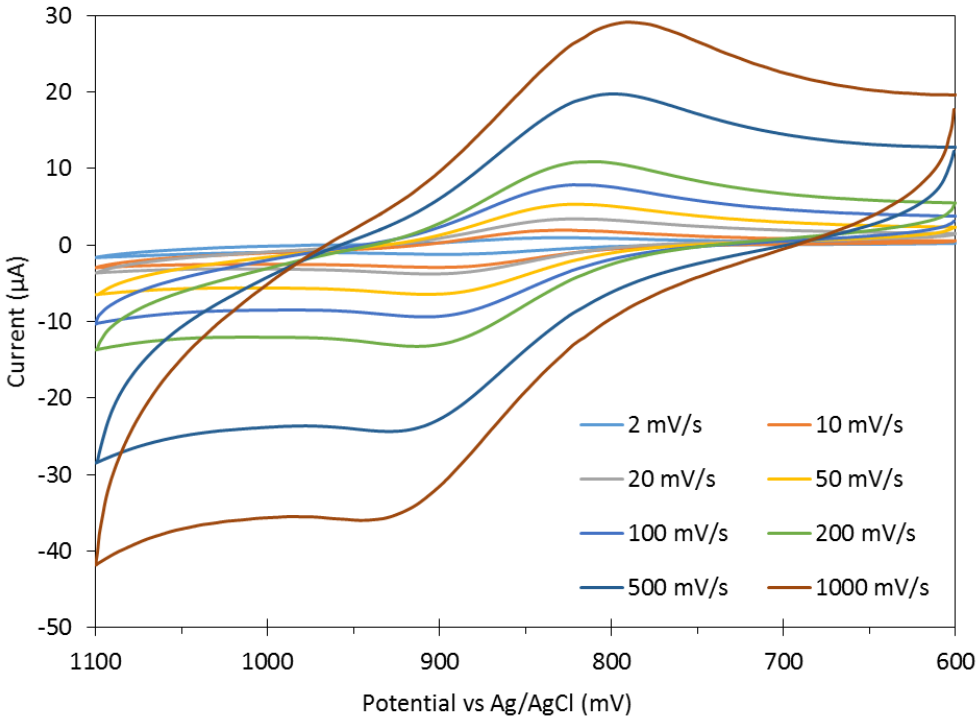

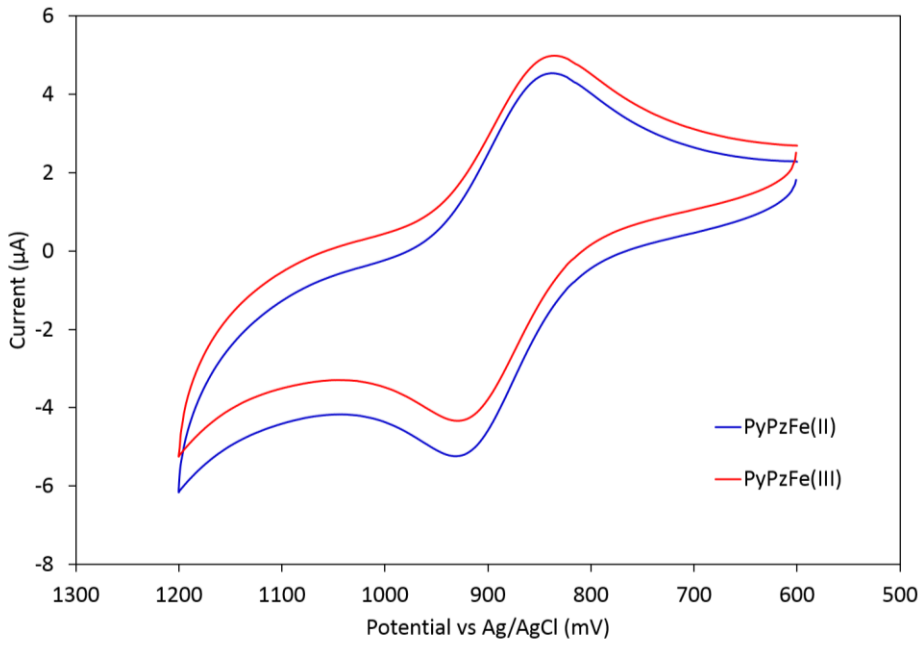

Figure S6. (Upper) Cyclic voltammetry of 1 mM (PyPz)Fe^{II} in pH 2.2 100 mM NaPi buffer at different scan rates at 25 °C. E_{pa}, E_{pc}, $E_{1/2}$ and ΔE values from the data are listed in **Table S1**. (Lower) Comparison of cyclic voltammetry of **1** and **2**.

Table S1. Cyclic voltammetry parameters of **1**/**2** couple

Scan rate (mV/s)	**E_{pa} (mV vs Ag/AgCl)**	**E_{pc} (mV vs Ag/AgCl)**	**$E_{1/2}$ (mV vs Ag/AgCl)**	**ΔE (mV)**
2	898	830	864	68
10	902	828	865	74
20	905	822	863.5	83
50	908	821	864.5	87
100	909	823	866	86
200	913	812	862.5	101
500	930	799	864.5	131
1000	945	790	867.5	155

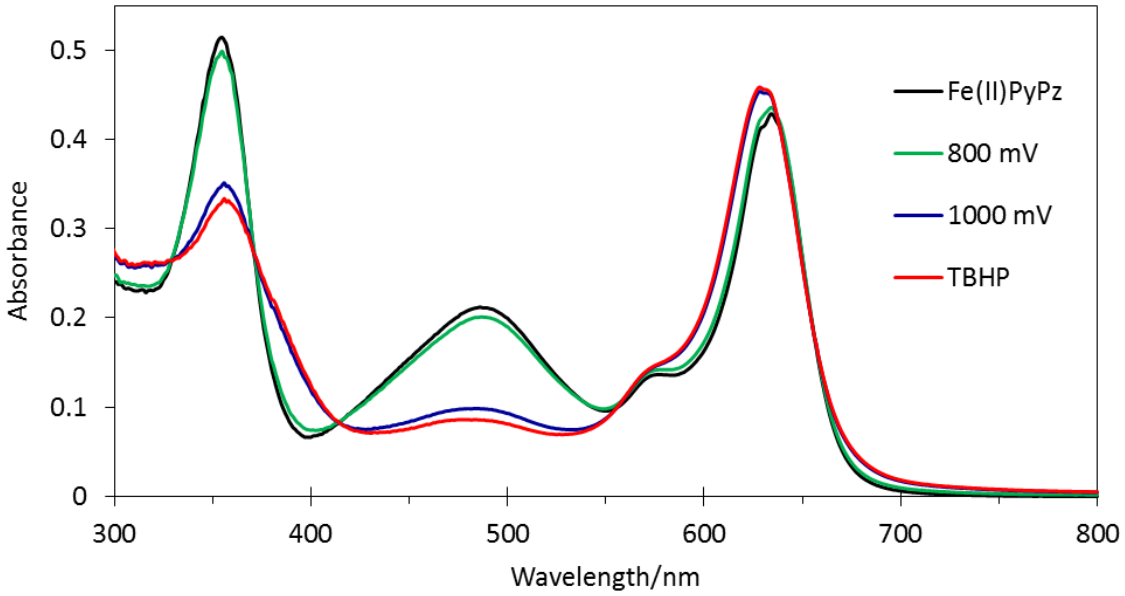

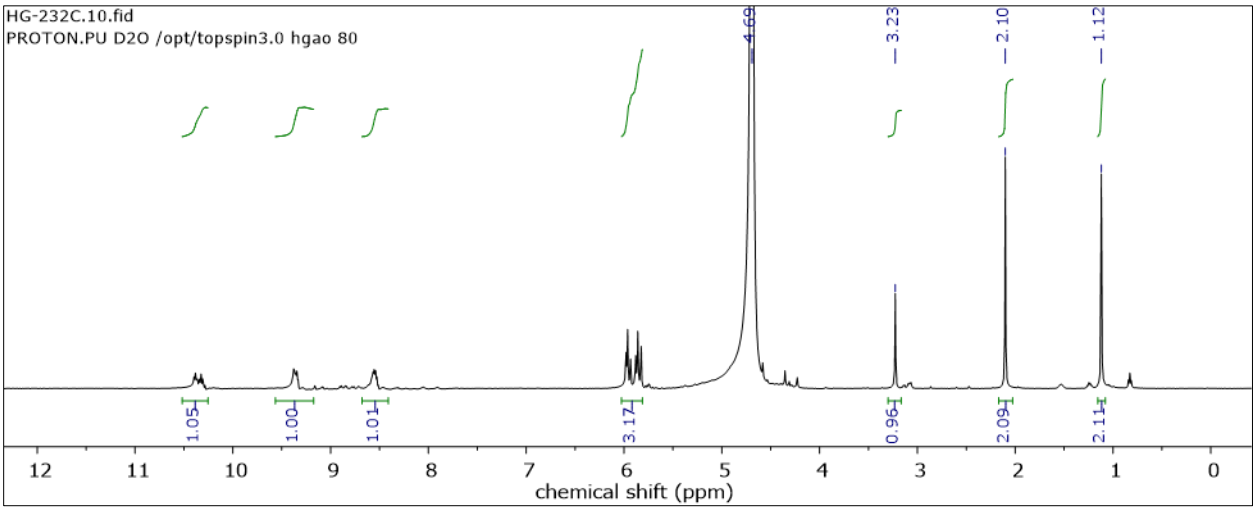

Figure S7. (Upper) UV-vis spectra of 11 μM (PyPz)Fe in 100 mM NaPi buffer at pH = 2.2. The black line shows the spectrum of (PyPz)Fe^{II} (**2**). The green line is bulk electrolysis of **2** at 800 mV vs Ag/AgCl. The blue line is bulk electrolysis of **2** at 1000 mV vs Ag/AgCl, which yields (PyPz)Fe^{III} (**1**). The red line is the spectrum after adding 1 equiv of *t*-butyl hydroperoxide (TBHP) to **2**, which also produced **1**. (Lower) ^{1}H NMR (500 MHz) of the reaction of **2** with 2.2 eq TBHP in D_2O (NMR was taken after **1** had decayed back to **2.** The NMR of paramagnetic **1** was broad and featureless. In addition to **1**, oxidation of **2** with TBHP also generated methanol (3.23 ppm, 1.3 equiv) and acetone (2.10 ppm, 1.3 equiv) in a 1:1 ratio, as determined by integration of the NMR signals. *Tert*-butyl alcohol (1.12 ppm, 0.9 equiv) was also observed as byproduct. The result is consistent with a one-electron oxidation of **2**.

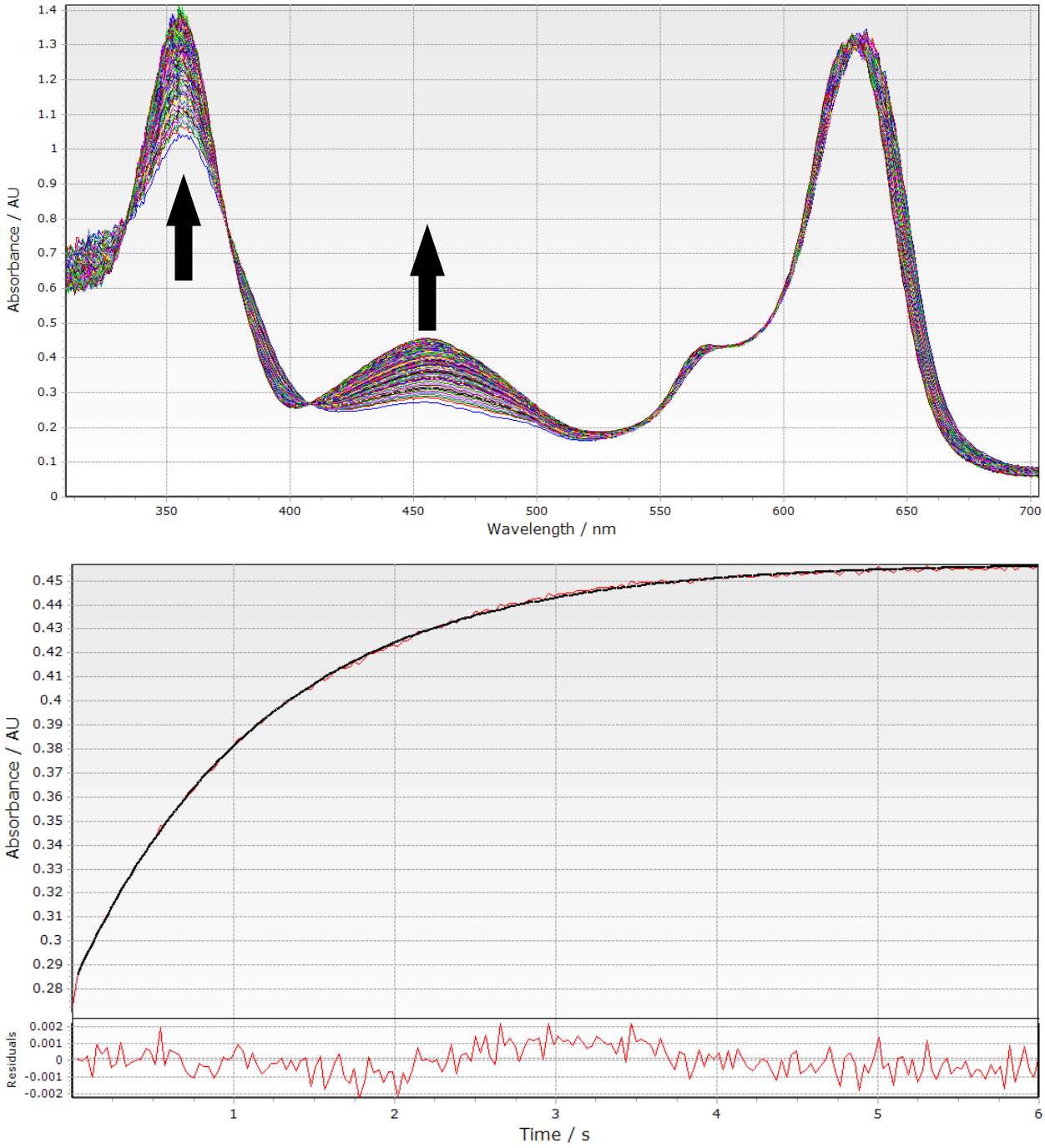

Figure S8. Single-mixing, stopped-flow experiment for xanthene reaction with (PyPz)Fe^{III}–OH (**1**). Conditions: pH 2.2 100 mM NaPi buffer / acetonitrile = 50/50 (v/v) solution, T = 20.0 ºC, [xanthene] = 6 mM, [(PyPz)Fe] = 0.16 mM. Total time = 6 s. 200 scans, 30 ms/scan. (Top) Diode array spectra of the stopped-flow experiment. (Bottom) Change in absorbance at 455 nm was plotted over time (red line). Fitting these data to a single exponential equation (black line) resulting in a pseudo-first order rate constant of 0.879 ± 0.003 s^{-1} (R^2 = 0.9996). SVD analysis of the data gave similar results. Difference in absorbance of fitted black curve and measured red curve was labelled as residuals in the bottom.

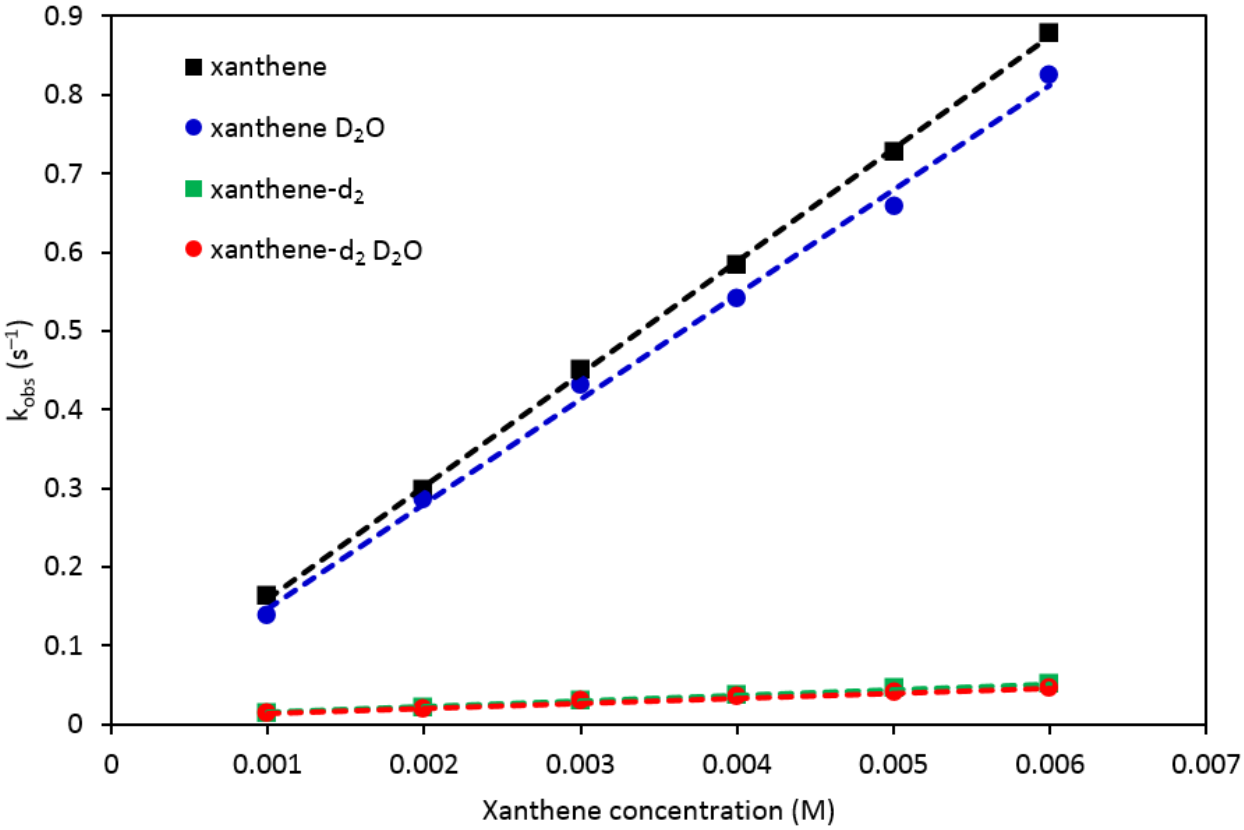

Figure S9. C–H abstraction of xanthene by **1** under pseudo first-order conditions. T = 20.0 °C. **1** was generated by bulk electrolysis at 1000 mV vs Ag/AgCl in pH 2.2 100 mM NaPi buffer. Rates are measured by single-mixing stopped-flow experiments. Reaction with proteo xanthene in proteo NaPi buffer (with 50% acetonitrile to increase solubility, pH of the mixture is 3.0) yields a bimolecular rate constant of 142.9 ± 1.2 M^{-1} s^{-1} (R^2 = 0.9996) (black). Xanthene-d_2 gave a much slower bimolecular rate constant of 7.32 ± 0.20 M^{-1} s^{-1} (R^2 = 0.996), which yields a substrate KIE of 19.5 ± 0.6 (green). Reaction of (PyPz)Fe^{III}–OD with proteo xanthene in deuterated buffer (pD 2.2 before mixing with CH_3CN) shows a slightly slower bimolecular rate constant than in the proteo buffer case, 133.1 ± 3.8 M^{-1} s^{-1} (R^2 = 0.996), which yields a solvent KIE of 1.07 ± 0.03 (blue). Xanthene-d_2 in D_2O afforded a bimolecular rate of 6.47 ± 0.38 M^{-1} s^{-1} (R^2 = 0.983), indicating a combined substrate-solvent isotope effect of 22.1 ± 1.3 (red).

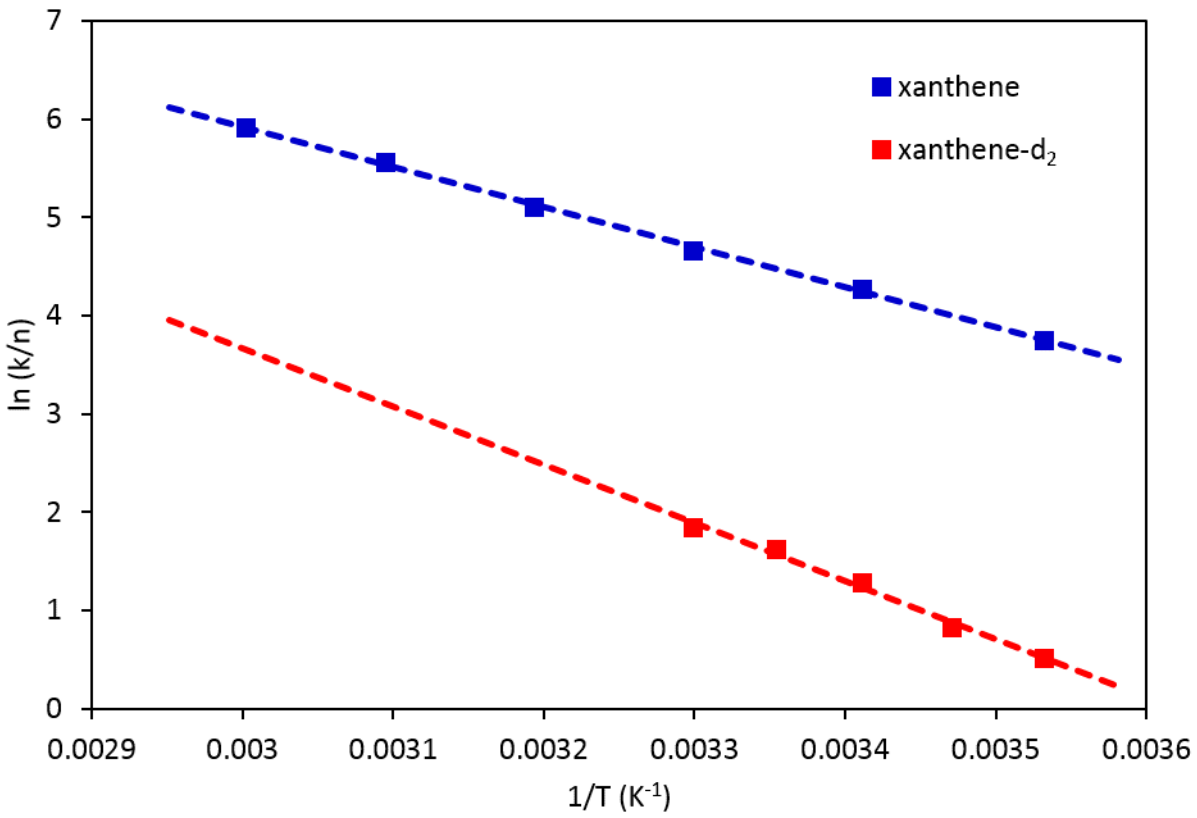

Figure S10. Arrhenius plot of xanthene and xanthene-d_2 oxidation by **1** in pH 2.2 100 mM NaPi buffer / acetonitrile = 50/50 (v/v) solution. Blue squares are xanthene data which gives E_a(H) = 8.1 ± 0.1 kcal mol^{-1} and ln A(H) = 18.16 ± 0.22 (R^2 = 0.999). Red squares show the result from xanthene-d_2 which gives E_a(D) = 11.8 ± 0.6 kcal mol^{-1} and ln A(D) = 21.41 ± 1.09 (R^2 = 0.991). $\Delta E_a = E_a(D) - E_a(H)$ = 3.7 ± 0.6 kcal mol^{-1}. A(H) / A(D) = 0.04.

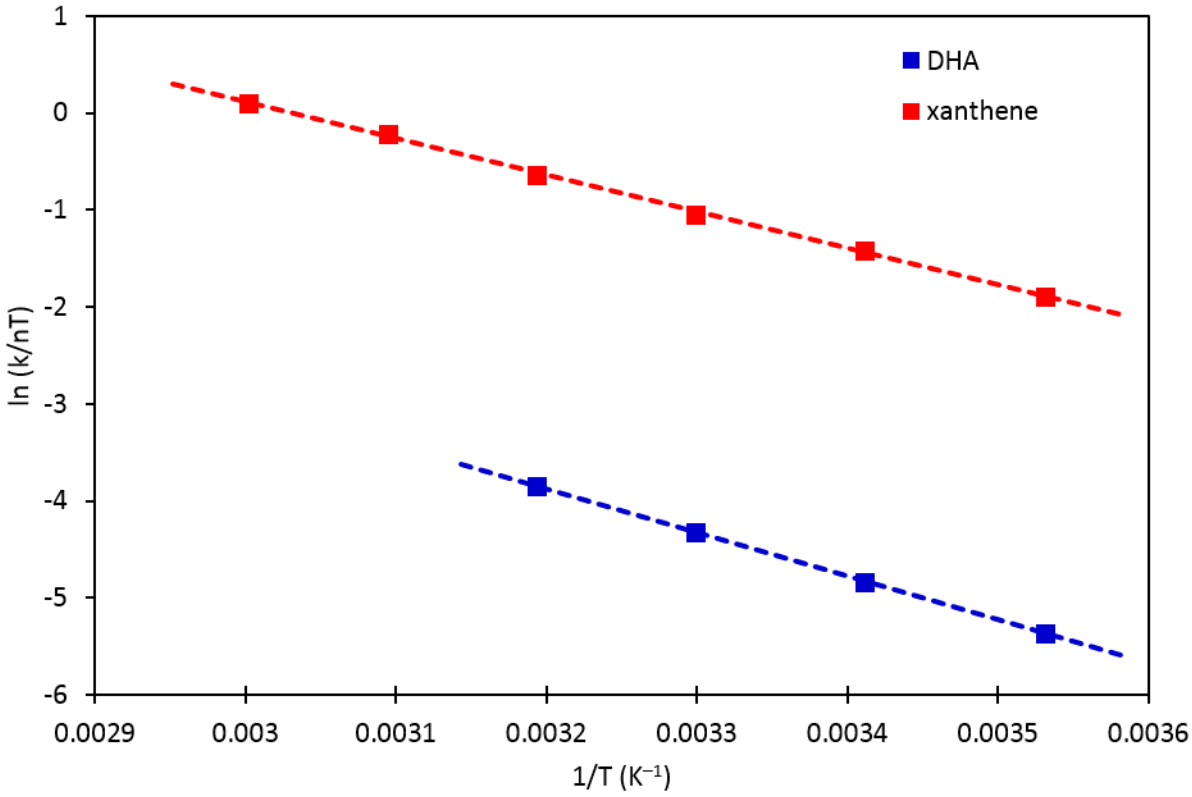

Figure S11. Eyring plot for the reduction of **1** by excess 9,10-dihydroanthracene (DHA, 283-313 K) and xanthene (283-333K) in 50:50 (v/v) pH = 2.2 0.1 M NaPi buffer/acetonitrile mixture. Xanthene: $\Delta H^{\ddagger}$ = 7.5 ± 0.1 kcal mol^{-1}, $\Delta S^{\ddagger}$ = –24.5 ± 0.4 cal mol^{-1} K^{-1}. DHA: $\Delta H^{\ddagger}$ = 8.9 ± 0.1 kcal mol^{-1}, $\Delta S^{\ddagger}$ = –26.4 ± 0.3 cal mol^{-1} K^{-1}.

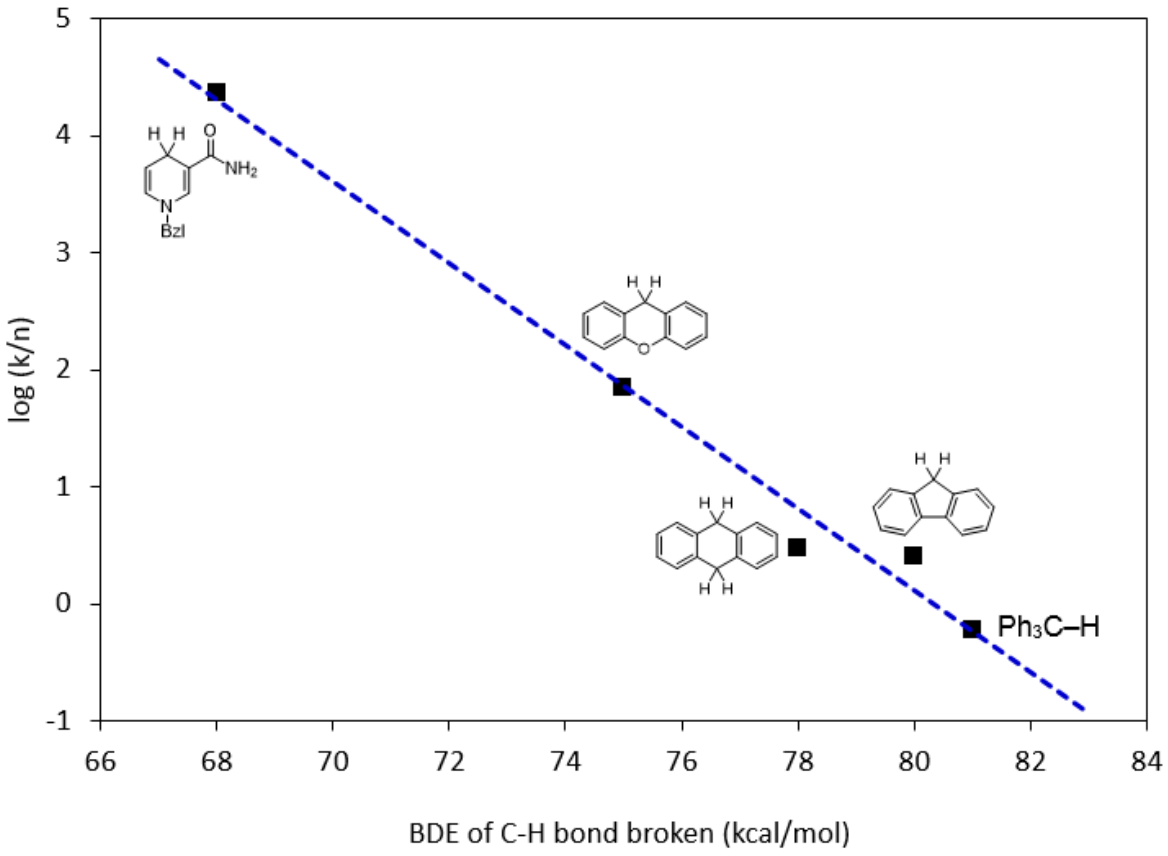

Figure S12. Plot of log (*k*/*n*) vs substrate bond dissociation energy (BDE), where *k* is the second-order rate constant and *n* is the number of equivalent C–H bonds which is broken in the reaction. Conditions: T = 20.0 °C, 50:50 (v/v) pH 2.2 0.1 M NaPi buffer/acetonitrile solution. Slope = –0.35 ± 0.03 (R^2 = 0.980).

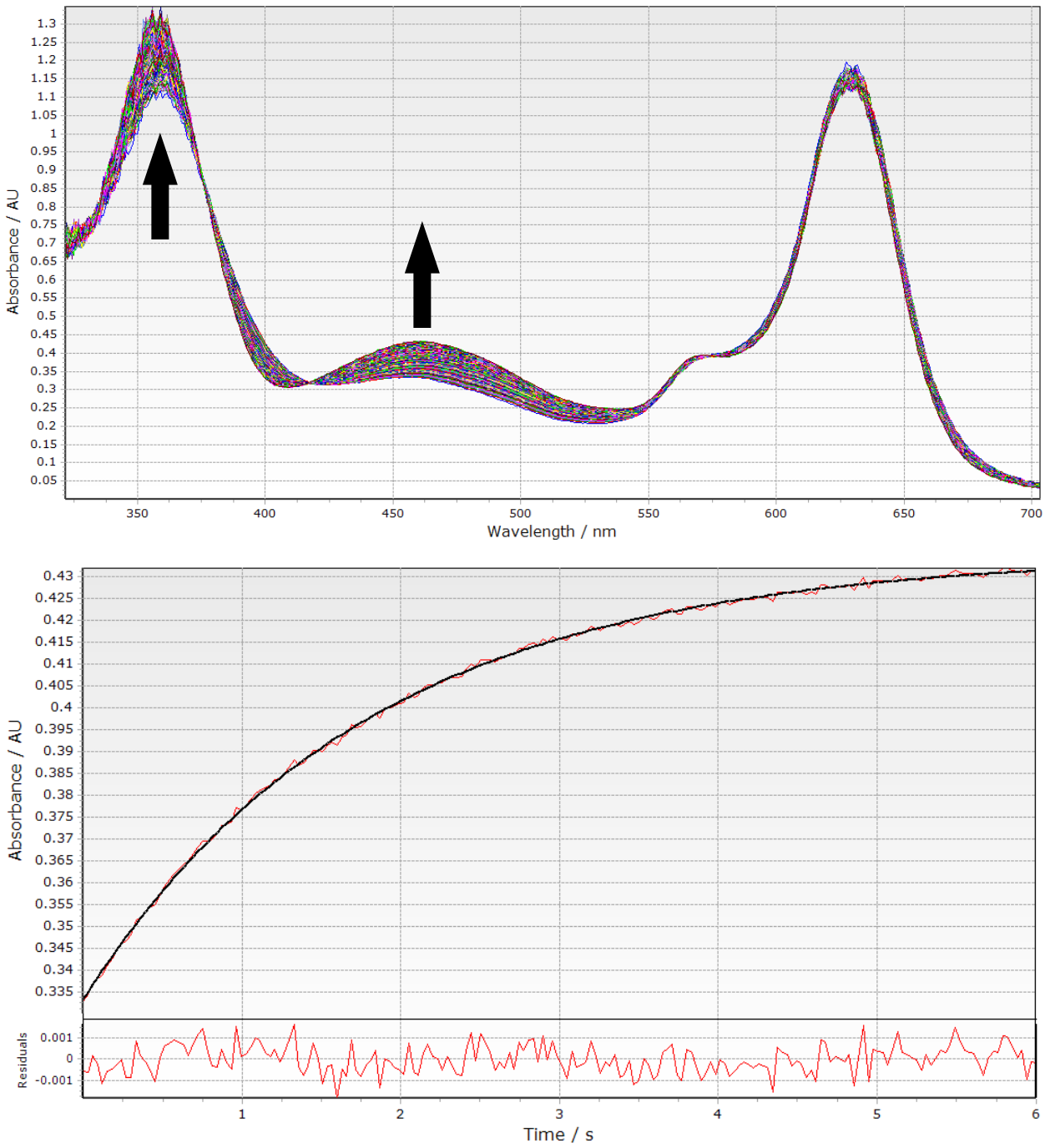

Figure S13. Single-mixing stopped-flow experiment of xanthene reacts with (PyPz)Fe^{III}–OH (**1**). Conditions: pH 6.2 100 mM NaPi buffer / acetonitrile = 50/50 (v/v) buffer, T = 20.0 °C, [xanthene] = 6 mM, [(PyPz)Fe] = 0.14 mM. Total time = 6 s. 200 scans, 30 ms/scan. (Top) Whole spectra of the stopped-flow experiment. (Bottom) Change in absorbance at 460 nm was plotted over time (red line). Fitting these data to a single exponential equation (black line) resulted in a unimolecular rate constant of 0.562 ± 0.003 s^{-1} (R^2 = 0.9994). Difference in absorbance of fitted black curve and measured red curve was labelled as residuals in the bottom.

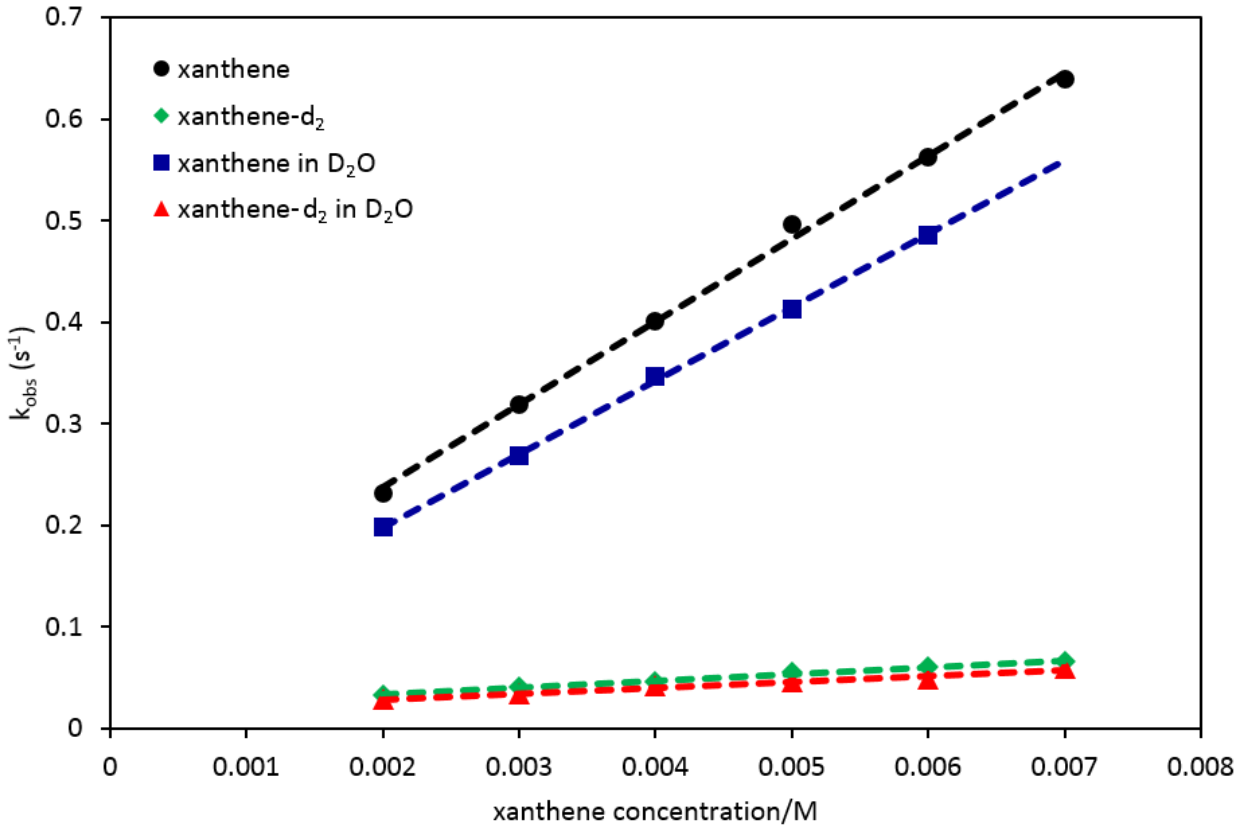

Figure S14. C–H abstraction of xanthene by **1** under pseudo first-order conditions. T = 20.0 °C. **1** was generated by bulk electrolysis at 700 mV vs Ag/AgCl in pH 6.2 100 mM NaPi buffer. Rates are measured by single-mixing stopped-flow experiments. Reaction with proteo xanthene in proteo NaPi buffer (with 50% acetonitrile to increase solubility, pH of the mixture is 7.0) yields a bimolecular rate constant of 81.7 ± 1.9 M^{-1} s^{-1} (R^2 = 0.997) (black). Xanthene-d_2 gives a much slower bimolecular rate constant of 6.68 ± 0.19 M^{-1} s^{-1} (R^2 = 0.996), which yields a substrate KIE of 12.2 ± 0.4 (green). Reaction of (PyPz)Fe^{III}–OD with proteo xanthene in deuterated buffer (pD 6.2 before mixing with CH_3CN) shows a slightly slower bimolecular rate constant than in the proteo buffer case, 72.1 ± 1.0 M^{-1} s^{-1} (R^2 = 0.999), which yields a solvent KIE of 1.13 ± 0.03 (blue). Xanthene-d_2 in D_2O afforded a bimolecular rate of 5.72 ± 0.39 M^{-1} s^{-1} (R^2 = 0.982), indicating a combined substrate-solvent isotope effect of 14.3 ± 1.0 (red).

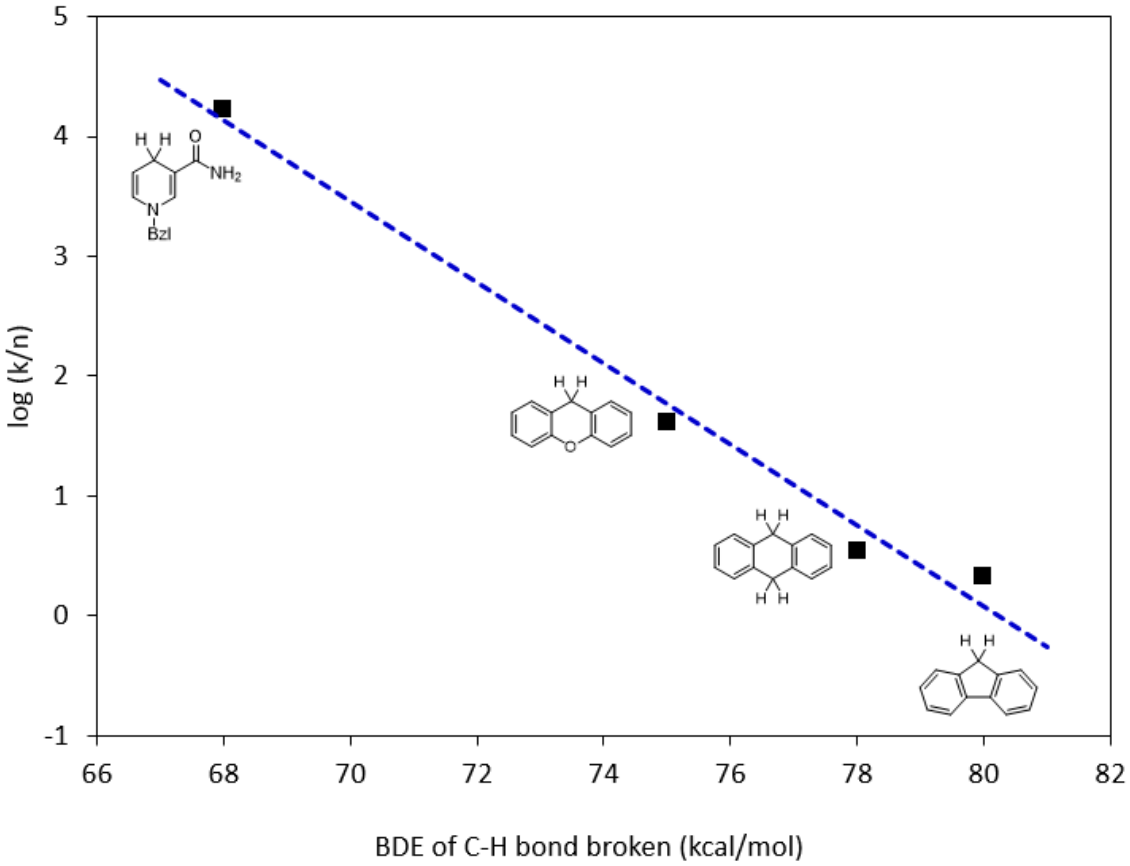

Figure S15. Plot of log (*k*/*n*) vs substrate bond dissociation energy (BDE), where *k* is the second-order rate constant and *n* is the number of equivalent C–H bonds which is broken in the reaction. Conditions: T = 20.0 °C, 50:50 (v/v) pH 6.2, 0.1 M NaPi buffer/acetonitrile solution. Slope = –0.34 ± 0.03 (R^2 = 0.978).

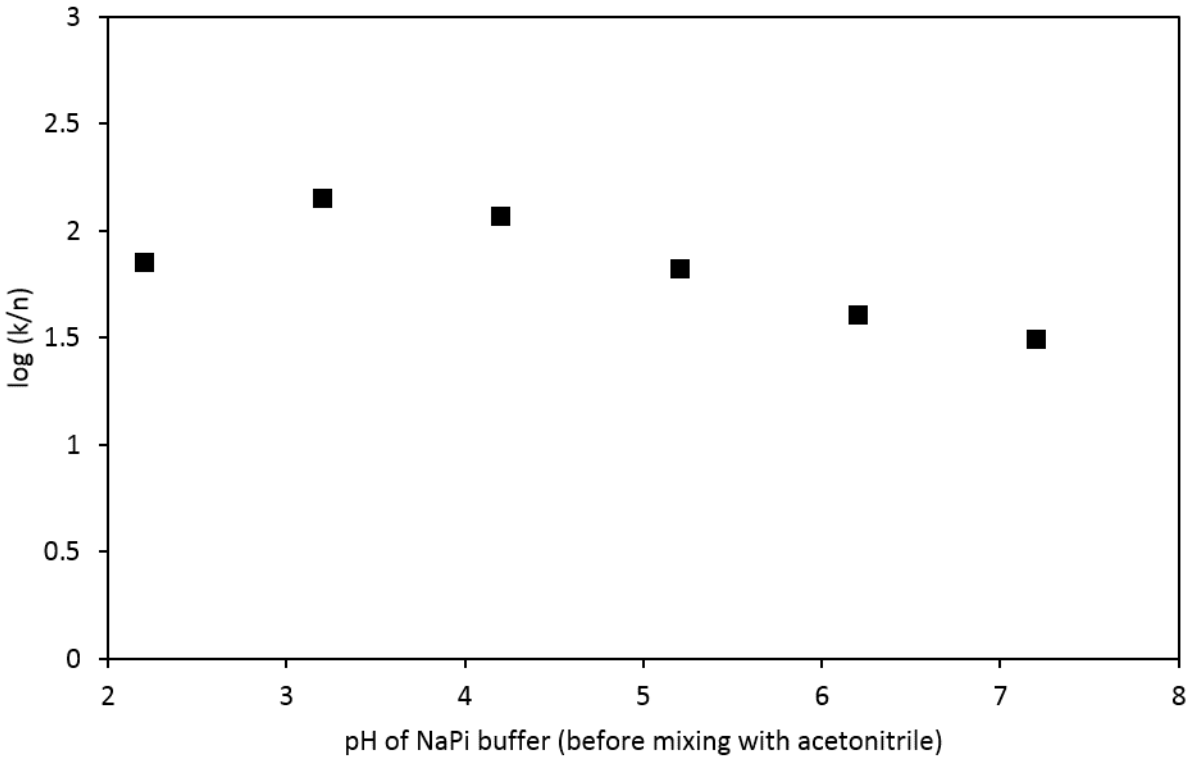

Figure S16. Reaction of xanthene with **1** vs. pH. Second-order rate constants are all within 0.7 orders of magnitude over the pH range from 2.2 to 7.2. Reaction conditions: **1** was generated by electrolysis at 1000 mV (vs Ag/AgCl) for pH 2.2, 940 mV for pH 3.2, 880 mV for pH 4.2, 820 mV for pH 5.2, 760 mV for pH 6.2, 700 mV for pH 7.2. T = 20 °C. 50/50 (v/v) 100 mM NaPi buffer/acetonitrile solution.

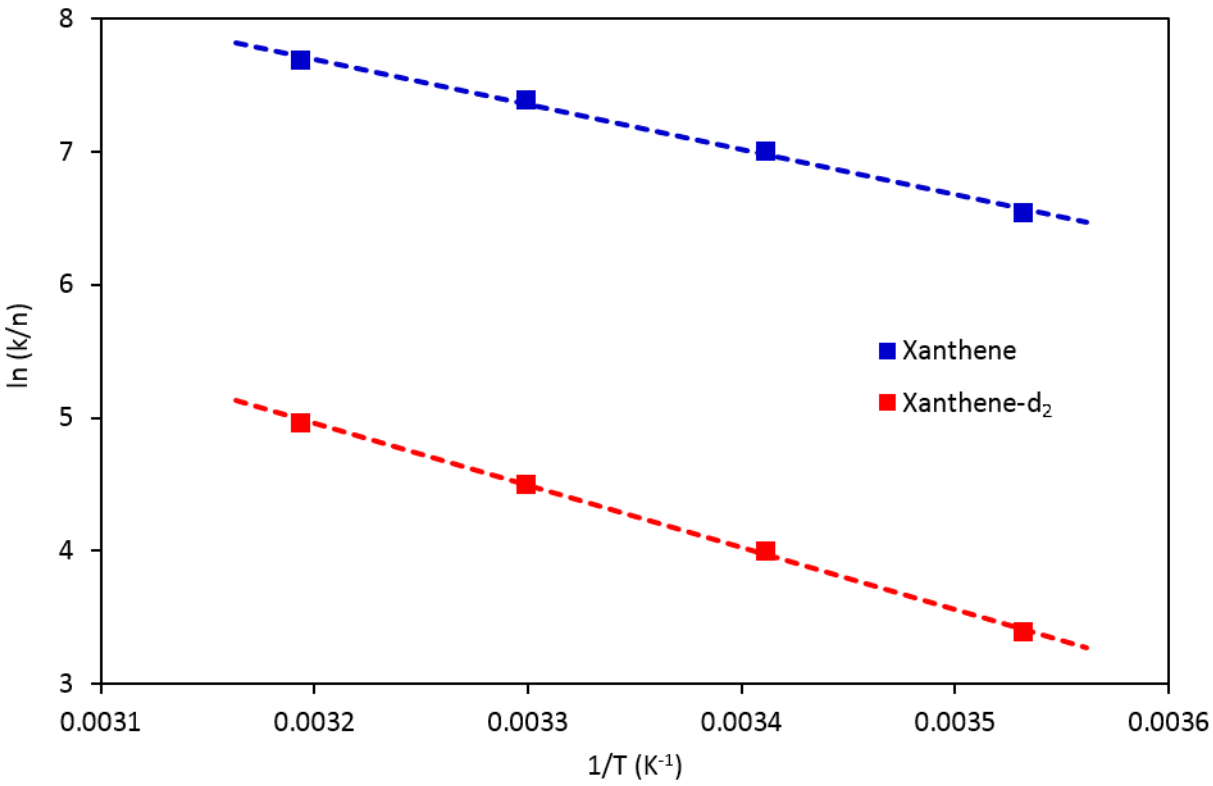

Figure S17. Arrhenius plot for xanthene and xanthene-d_2 oxidation by **1** in 6 mM $HClO_4$ (pH 2.2) aqueous acetonitrile = 50/50 (v/v) solution. Blue squares are xanthene data which gives E_a(H) = 6.73 ± 0.33 kcal mol^{-1} and ln A(H) = 18.53 ± 0.55 (R^2 = 0.993). Red squares show the result from xanthene-d_2 which gives E_a(D) = 9.23 ± 0.23 kcal mol^{-1} and ln A(D) = 19.81 ± 0.38 (R^2 = 0.998). $\Delta E_a = E_a(D) - E_a(H)$ = 2.5 ± 0.4 kcal mol^{-1}. A(H) / A(D) = 0.28 ± 0.14.

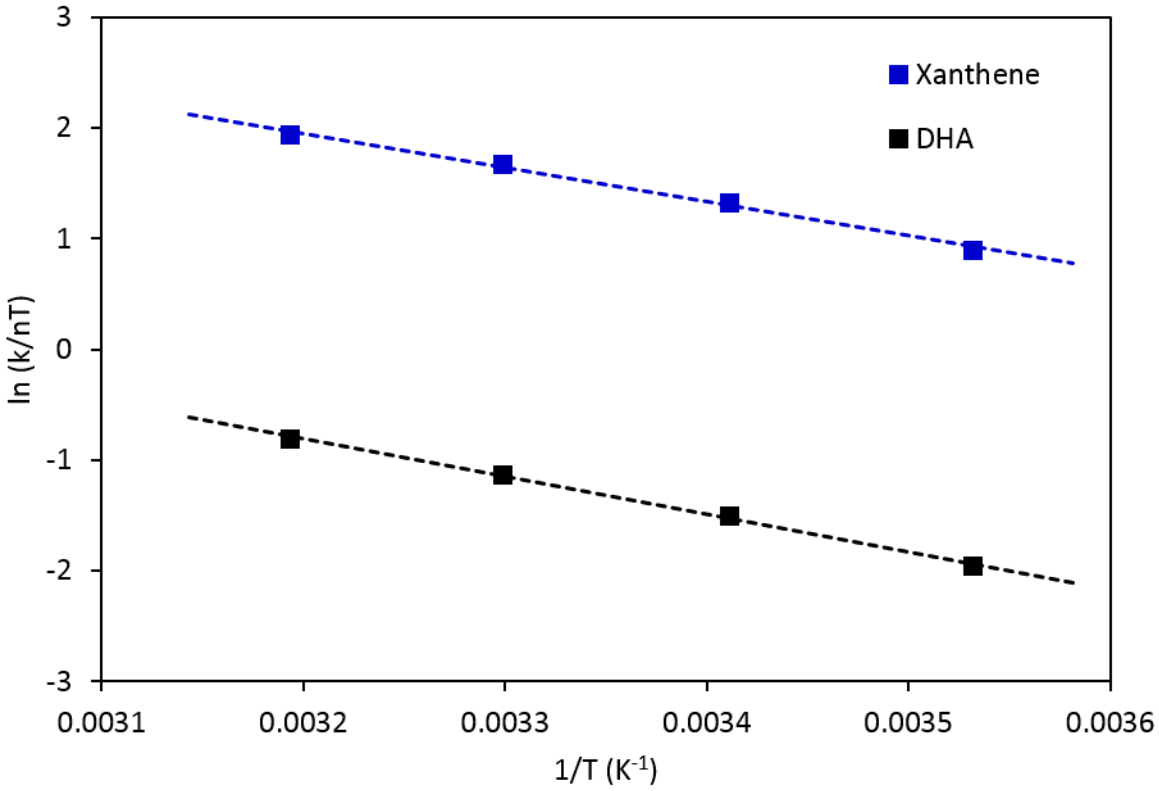

Figure S18. Eyring plot of xanthene and 9,10-dihydroanthracene oxidation by **1** in 50:50 (v/v) 6 mM $HClO_4$ (pH 2.2) water/acetonitrile solution at 283-313 K. Blue squares are xanthene data which give $\Delta H^{\ddagger}$ = 6.1 ± 0.3 kcal mol^{-1} and $\Delta S^{\ddagger}$ = –23.7 ± 1.1 cal mol^{-1} K^{-1}. Black squares are DHA data which give $\Delta H^{\ddagger}$ = 6.8 ± 0.3 kcal mol^{-1} and $\Delta S^{\ddagger}$ = –27.2 ± 0.8 cal mol^{-1} K^{-1}.

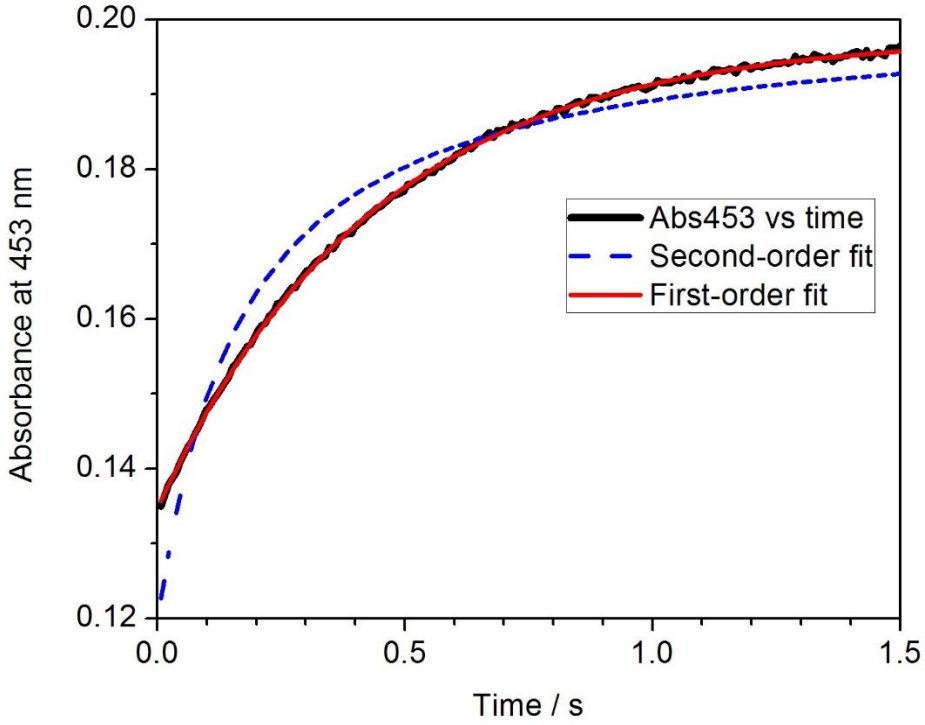

Figure S19. Experimental data from Figure 1A (black solid line), first-order fit (red solid line) and second-order fit (blue dashed line). First-order fit gives $R^2 = 0.9997$. Second-order fit gives $R^2 = 0.955$.

Table S2. Thermodynamic and Kinetic Parameters for **1** and Selected Metal Oxo/Hydroxo Complexes

Complex	O-H BDE (kcal/mol)	log (k_{DHA}/4)	$\Delta H^{\ddagger}$ (kcal/mol)	$\Delta S^{\ddagger}$ (eu)	KIE	BEP slope	Ref
$[(PyPz)Fe^{III}(OH)(OH_2)]^{4+}$	84	1.91	6.8(3)	–27(1)	20 (xanthene) 21 (DHA) 24 (fluorene)	–0.35	This work
$[Fe^{III}(\mathbf{PY5})(OMe)]$-$(OTf)_2$	83.5	–3.10	13.4(5)	–25(3)	5.5	–0.21	7a, 7b
$[Fe^{III}(\mathbf{PY5})(OH)]$-$(OTf)_2$	80	–3.37	13.2(5)	–26(5)	6.3	–0.19	7d
$[Mn^{III}(\mathbf{PY5})(OH)]$-$(OTf)_2$	82	–2.80	9.3(5)	–36(5)	2.4	–0.06	7c
$[Fe^{III}(Hbim)(H_2bim)_2]$-$(ClO_4)_2$	76	–4.50	11.6(5)	–36(5)	4.0 (313 K)	–0.20	26d
$[L_2Mn^{IV}(O)_2Mn^{III}L_2]^{3+}$	79	–3.41	14.5(10)	–23(3)	4.2	NA	26c
$[L_2Mn^{III}(O)(OH)Mn^{III}L_2]^{3+}$	75	–3.98	16.0(10)	–21(3)	NA	NA	26c
$LCu^{III}OH$	90	2.27	5.4(2)	–30(2)	29	–0.27	10
$Fe^{IV}(O)$TPFPP	~82	0.54	NA	NA	20	–0.22	6k
$Fe^{IV}(O)(TBP_8Cz^{+}\cdot)$	~81	0.11	xanthene 12.7(8)	xanthene -9(3)	5.7 (xanthene)	–0.42	6c
$[Fe^{IV}(O)(N4Py)]^{2+}$	78	0.65	NA	NA	50 (PhEt)	–0.19	6a, 18
$Fe^{IV}(O)$(TMC)X	84	–0.10	NA	NA	10	–0.38	26g
$Fe^{IV}(O)$TMP	88	0.64	NA	NA	NA	–0.31	26h